J Nanopart Res (2014) 16:2803
DOI 10.1007/s11051-014-2803-6

RESEARCH PAPER

Cubic superparamagnetic nanoparticles of $NiFe_2O_4$ via fast microwave heating

W. S. Galvão · R. M. Freire · T. S. Ribeiro · I. F. Vasconcelos · L. S. Costa · V. N. Freire · F. A. M. Sales · J. C. Denardin · P. B. A. Fechine

Received: 19 May 2014 / Accepted: 8 December 2014 / Published online: 23 December 2014

Abstract This study demonstrated the possibility of using microwave heating as a fast and cheap method for synthesizing superparamagnetic nanoparticles. In this sense, $NiFe_2O_4$ samples were subjected to microwave heating at various temperatures to determine the lowest temperature at which the crystalline phase of the nanoparticles occurs. X-Ray powder diffraction, ^{57}Fe Mössbauer spectroscopy, and transmission electron microscopy of the samples were performed to confirm the formed nanoparticles. It was observed a cubic structure of inverse spinel type with good crystallinity. The magnetic properties of the samples were studied using a vibrating sample magnetometer and was found to zero values to remanent magnetization and coercivity field. This behavior suggests superparamagnetic features for all samples. The crystallite size (9, 10, and 12 nm) and saturation magnetization (31–45 emu/g) were used as a function of the increase of the temperature treatment time. Blocking temperature was found by tracing remanent magnetization versus temperature.

Keywords Ferrites · Magnetic nanoparticles · Hydrothermal synthesis · Microwave Heating

W. S. Galvão · R. M. Freire · P. B. A. Fechine (✉)
Grupo de Química de Materiais Avançados (GQMAT), Departamento de Química Analítica e Físico-Química, Universidade Federal do Ceará–UFC, Campus do Pici, CP 12100, Fortaleza, CE CEP 60451-970, Brazil
e-mail: fechine@ufc.br

T. S. Ribeiro · I. F. Vasconcelos
Departamento de Engenharia Metalúrgica e de Materiais, Universidade Federal do Ceará, Fortaleza, CE, Brazil

L. S. Costa
Department of Inorganic Chemistry, Institute of Chemistry, State University of Campinas–UNICAMP, CP 6154, Campinas, SP CEP 13083-970, Brazil

V. N. Freire · F. A. M. Sales
Departamento de Física, Centro de Ciências, Universidade Federal do Ceará, Campus do Pici, Caixa Postal 6030, Fortaleza, CE 60455-760, Brazil

J. C. Denardin
Departamento de Física, Universidad de Santiago de Chile, USACH, Av. Ecuador, Santiago 3493, Chile

Introduction

In recent decades, magnetic nanoparticles have been the subject of extensive studies due to its peculiar characteristic of interacting with an external magnetic field (Zhang et al. 2012). In the case of ferrimagnetic nanoparticles by applying a magnetic field on them, the spins of the electrons of the material align in favor of the field, resulting in an attraction force. This property gives it an important capability to transport operations and separation (Latham and Williams 2008). When dealing with biomedical applications it is necessary to observe some essential requirements, among it, the superparamagnetism. In a brief description, we can call

superparamagnetism, as the presence of magnetism in a material, only when it is subjected to the magnetic field, the effect ceases as soon as removed the external magnetic field (Petcharoen and Sirivat 2012). An effect is provided by superparamagnetism, which prevents agglomeration of the particles after removal of the external magnetic field. The particles based on iron oxide are known as ferrites and represent more nanomaterials used for biomedical applications. An example of magnetic material would be nickel ferrite ($NiFe_2O_4$). It is a typical ferrimagnetic material which completely crystallizes inverse spinel-type structure, with all nickel ions in octahedral sites located while the iron ions occupy tetrahedral and octahedral sites (Karakas et al. 2013). After magnetite (Fe_3O_4), nickel ferrite is the one with the highest saturation magnetization (M_S). A difficulty presented for the acquisition of these materials has been the process of synthesis. Unlike magnetite, which forms a crystalline phase at room temperature, the ferrites of the type MFe_2O_4, where M can be a transition metal such as Co^{2+}, Ba^{2+}, Mn^{2+}, Zn^{2+}, and Ni^{2+} (Klabunde and Richards 2001), not the crystalline phase precipitated at low temperatures, necessitating the provision of large amounts of heat over long periods of time. Temperatures and heating times used vary widely according to the methodology used for the synthesis.

Some studies have shown that the use of temperatures around 160 °C for 6 h using the hydrothermal method (Zhang et al. 2013), 650 °C by sol–gel auto-combustion process (Tong, Cai et al. 2013), and temperatures about 800 °C for 1.5 h by ball milling method (Zhang et al. 2010) are nedeed to obtain magnetic nanoparticles. There is an increasing demand for alternatives to the synthesis of these materials, which provide superior properties when compared with those available from conventional methods. However, the microwave-assisted synthesis of nanomaterials is gaining much interest among researchers due to their unique characteristics such as short reaction time, rapid volumetric heating, energy saving, and abrupt rise in temperature until the level synthesis (Koziej et al. 2013). In this work, $NiFe_2O_4$ superparamagnetic nanoparticles were synthesized by co-precipitation method and assisted by microwave heating. Three samples were prepared at 160 °C and at three different heating times in order to observe the influence of heating on the structure and magnetic properties. The samples were investigated using X-Ray powder diffraction (XRPD), 57Fe Mössbauer spectroscopy, transmission electron microscopy (TEM), and Magnetic Measurements. The synthesis and study of these superparamagnetic nanoparticles are important due to their possible applications in magnetic separation, ferrofluids, magnetic hyperthermia, etc.

Experimental

Materials and methods

All reagents were commercial products with analytical grade without further purification. The chemical reagents for this work were $FeCl_3.6H_2O$ (Dinâmica, 97 %), $NiCl_2.6H_2O$ (Vetec, 97 %), sodium hydroxide (Cinética Química, 97 %), and solution of HCl 5 %.

Synthesis of $NiFe_2O_4$ superparamagnetic nanoparticles

In the co-precipitation route, metallic salts containing Ni^{2+}/Fe^{3+} were dissolved and mixed in Milli-Q water in the molar ratio of 1:2 to form the spinel-phase $NiFe_2O_4$. The aqueous mixture was heated to 50 °C, and 20 ml of a solution of NH_4OH was added dropwise with vigorous stirring. The precipitate was taken to microwave heating at 160 °C for 7, 12, and 17 min, labeled as Ni-7, Ni-12, and Ni-17 min, respectively. All the microwave-assisted hydrothermal reactions were carried out in a microwave-accelerated reaction system, MARS-5 (CEM, USA). This system operated at 2.45 GHz frequency with a power of 200 W. It was controlled by temperature or pressure (200 psi) or a standard control, using a ramp program of temperature. Some experiments were tested to determine the best conditions to obtain the nanoparticle considering better crystallinity of the sample and less synthesis temperature. The precipitate was washed several times with Milli-Q water until the residual solution became neutral. Finally, the magnetic nanoparticles were dried. The chemical reaction may be written as Eq. 1.

$$Ni^{2+} + 2Fe^{3+} + 8OH^{-} \rightarrow NiFe_2O_4 + 4H_2O \quad (1)$$

Characterization of nanoparticles

XRPD

The structural analysis and verification of single-phase nature of the samples were performed using XRPD. These measurements were carried out using Rigaku X-ray diffractometer equipped with CoKα radiation tube (1.7889 Å) operated at a voltage of 30 kV and a current of 15 mA. The phase identification analysis was performed by comparing powder diffractograms with standard patterns from International centre for diffraction data (ICDD). Rietveld refinement procedure (Rietveld 1967) was applied to all diffraction patterns using the DBWS 2.25 (Bleicher, Sasaki et al. 2000). The crystallite sizes of nanoparticles were calculated from the XRPD data using Scherrer's equation (Patterson 1939).

^{57}Fe Mössbauer spectroscopy

The Mössbauer spectrum was recorded at room temperature (300 K) from *FAST (ConTec) Mössbauer System* spectrometer using transmission geometry. A ^{57}Co radioactive source was used. The data analysis was performed using NORMOS program written by R. A. Brand (distributed by Wissenschaftliche Elektronik GmbH, Germany). Isomer shifts (δ) are referred as α-Fe at room temperature.

Magnetic measurements

The magnetic measurements were obtained using a vibrating sample magnetometer brand cryogenic VSM 5 Tesla system with a magnetic field of five Tesla and even the temperature range of 2–300 K. The VSM has been previously calibrated using a pure Ni wire, and after measuring the mass of each sample the magnetization was given in emu/g.

Transmission electron microscopy

Transmission electron microscopy (TEM) images were obtained using a JEOL JEM 2100 LaB6 operating at an accelerating voltage equal to 200 kV and equipped with a TV (Gatan ES500 W); CCD (TVips–16MP). TEM samples were prepared by drop casting a hexane dispersion of the nanocrystals onto carbon- and Formvar-coated copper grids. After deposition, the samples were dried to a temperature of 60 °C overnight prior to obtaining the images. The size distribution was determined by the measurement of 100 randomly selected particles in different regions of the expanding TEM images.

Results and discussion

In this study, it was possible to obtain a fast and cheap route to synthesize magnetic nanoparticles by microwave heating and using the lowest time and temperature. In this sense, $NiFe_2O_4$ phase was used for tests. For lower temperature, colloidal precipitates obtained in the hydrothermal synthesis were added to test tubes and subjected to heating at 130, 140, 150, and 160 °C (Fig. 1). The heating time was maintained constant in 7 min in all tests.

From the refinement of the data of XRPD, it was possible to identify a single phase for all samples (ICSD/PDF-08-4611). Table 1 summarizes the data obtained from Rietveld analysis and the main factors (S, Rwp). According to Fig. 1, the crystallographic planes belonging to the nickel ferrite appear at the temperature of 140 °C with little intensity. The sample synthesized at 150 °C presented low crystallinity

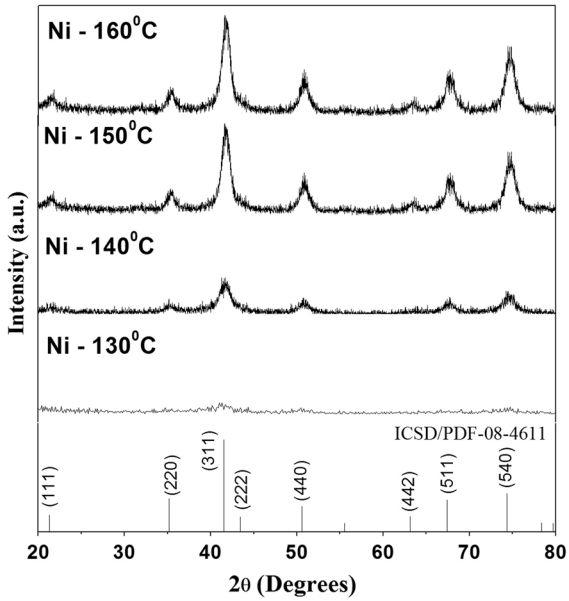

Fig. 1 XRPD of the $NiFe_2O_4$ nanoparticles synthesized at various temperatures

Table 1 Average crystallite sizes and microstrain percentage obtained by Scherrer and Williamson–Hall (W–H) models

Samples	Average crystallite sizes		Lattice parameter (Å), a=b=c	Microstrain (ε)	R_{WP} (%)	S
	Scherrer	W–H				
Ni-7 min	8.9	–	8.3434	0.63	19	1.11
Ni-12 min	9.8	9.8	8.3439	0.02	17	1.02
Ni-17 min	12.0	17.0	8.3555	0.17	14	1.07

according to the data obtained from refinements (Table 1). In contrast, the sample obtained at 160 °C presented high degree of crystallinity as shown by the data obtained from the refinement (Table 1) and TEM images (Fig. 3). These results suggest that the samples are constituted mainly by spinel phase. Due to this reason, this temperature was selected for the synthesis of other samples.

Several problems have been identified in attempts to achieve temperatures above 140 °C. It was observed with the leaking of the material caused by increased pressure inside the test tube, due to sudden increase in temperature characteristic of microwave heating. The ramp reached 80 °C during 30 s and continued increasing up to 100 °C, where it stays for a further 30 s, respectively, so until 160°C. The pressure and temperature were kept constant at 250 (psi) and 200 W, respectively.

A second experiment was conducted to study the influence of time of microwave heating on the physical and magnetic properties of nickel ferrite. Figure 2 shows the XRPD of the samples, and Table 1 exhibits the structural parameters obtained from the refinement. The diffraction patterns showed that all the peaks at 2θ of 21.5°, 29.9°, 35.3°, 41.7°, 54.1°, 56.8°, and 62.5° were corresponding to (111), (220), (311), (400), (422), (511), and (440) Bragg reflection, respectively. It can be well indexed to the inverse cubic spinel structure of NiFe2O4 (ICSD/PDF-08-4611) with spatial group Fd3 M (Barreto et al. 2011.). Rwp index was used to evaluate the quality of the refinement (Weidler et al. 1998) (Table 1).

The crystallite size was calculated using the Scherrer's equation, which relates the crystal size with the half-width of the diffraction peak (Braga et al. 2010), $t = \frac{0.9\lambda}{B\cos\theta_B}$, where t is the crystallite size average (Å), λ is the X-ray wavelength (1.7889 Å), and θ_B is the Bragg angle. The width of the peak (B) is obtained from the half-width of the peak height of the most

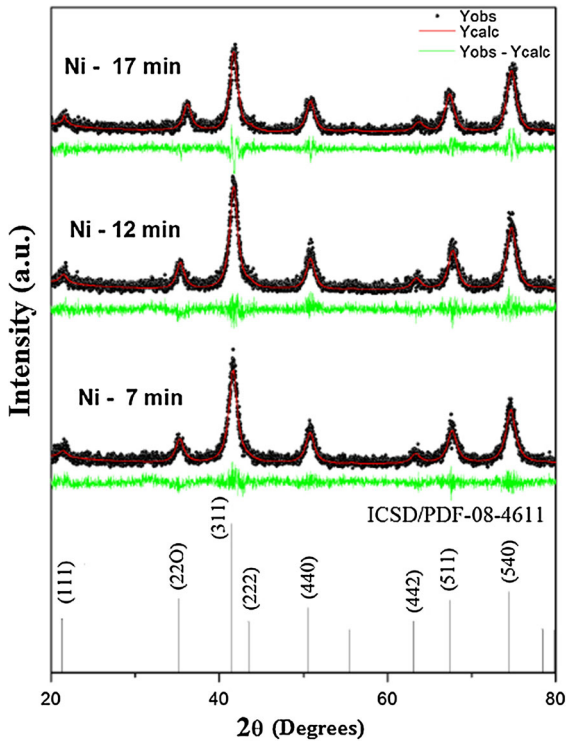

Fig. 2 XRPD of the $NiFe_2O_4$ magnetic nanoparticles at 160 °C in three different times of heating

intense diffraction. The values found for the crystallite size based on the widths of the main peak (311) were 8.9, 9.8, and 12 nm for samples Ni-7, Ni-12, and Ni-17 min, respectively. Therefore, it can be observed that an increase of the heating time produced an increase in crystal size, due to the greater diffusion of material to form larger particles (Bennett and Myers 1982). The surface of the particles is a region of high concentration of structural defects and broken links. In relation to the interior of the crystal structure, the surface energy is quite higher. It is precisely the possibility of reducing its total energy which causes the system to submit to reverse split. As the total area

of particle system is the sum of each one, it is possible to note that a lower energy of the system is assigned to a smaller surface area (Markov 1995). A search of a thermodynamic equilibrium leads to a process of nucleation and particle growth. This process is spontaneous and accelerated by increasing the temperature (Friedlander 2000).

Figure 3 shows the TEM micrograph of $NiFe_2O_4$ nanoparticles at 160 °C/12 min. Figure 3 a shows the measures of the spacing between the atomic planes which were calculated according to the equation: $d = \left(\sqrt{\frac{h^2}{a^2} + \frac{k^2}{b^2} + \frac{l^2}{c^2}}\right)^{-1}$, where a, b, and c are network parameters and h, k, and l are Miller indices. From these results, it was possible to relate the values to the distances measured from the TEM images and index them as the plane (220) to the family of planes of $NiFe_2O_4$ nanoparticles. The value found was equal to 0.296 nm. In the spinel structure, the integrated intensity of the (220) reflection depends exclusively on the cations occupying the tetrahedral sites (Thomas et al. 2013). In Fig. 3 b, it is possible to observe the arrangement of the atomic planes forming a structure of cubic morphology, indicating the high degree of crystallinity of the sample. Figure 3c shows the particle agglomeration state. This is a natural tendency for magnetic nanoparticles due to strong dipole–dipole attraction between the particles (Latham and Williams 2008). The histogram (Fig. 3 d) shows the crystal size distribution, with an average value of 8.2 nm. The size distribution was determined by the measurement of 100 randomly selected particles in different regions of the expanding TEM images. This result was consistent with the value obtained by Scherrer's equation and

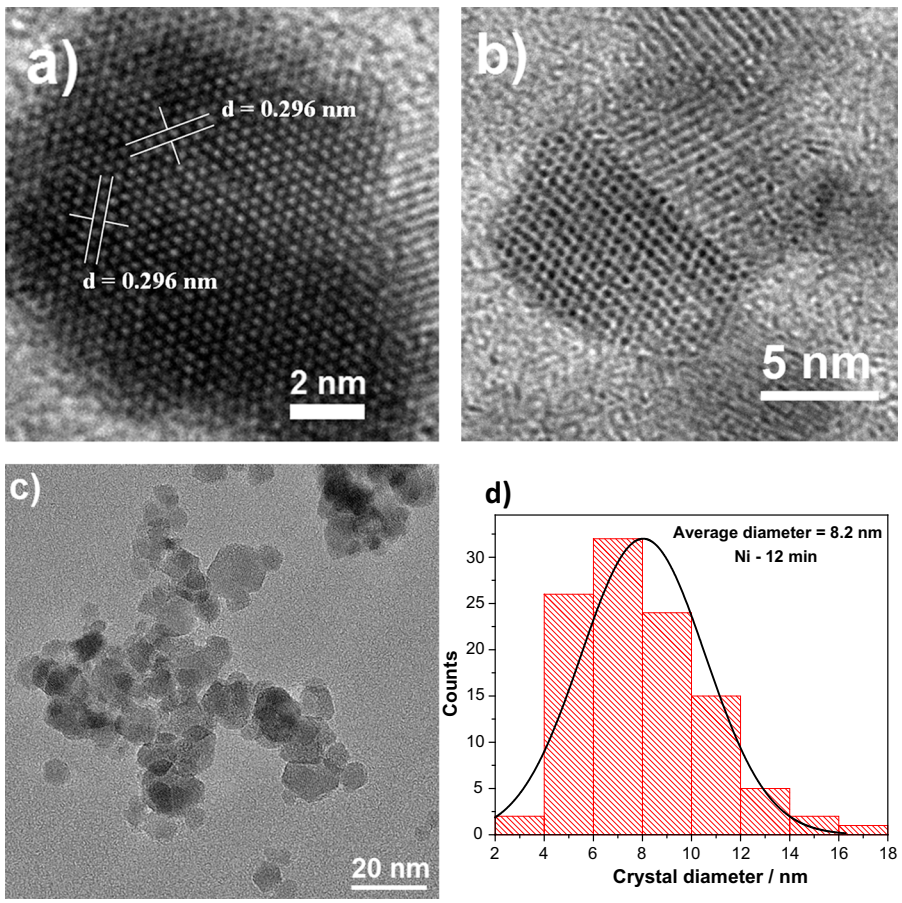

Fig. 3 TEM micrographs of the sample Ni-12 min: **a** spacing between planes which was indexed as (220) to the $NiFe_2O_4$ ferrite; **b** arrangement of the atomic planes forming a typical structure of the cubic ferrites; **c** clusters of nanoparticles and **d** average sizes presented in the histogram

demonstrates the proper refinement of data obtained from XRPD.

The growth of a crystal or the synthesis of a crystalline material may cause microdeformations in the structure, and this can result in variations in the lattice parameters of the unit cell. In this way, the Williamson–Hall method is used to extract structural parameters such as microstrain (the slope of the line), crystalline size (the linear coefficient of the straight line), and its homogeneity from angular widths of the diffraction peaks represented by the following equation (Williamson and Hall, 1953).

$$\frac{\beta.\cos\theta}{\lambda} = \frac{k}{D} + \frac{4\varepsilon}{\lambda} sen\theta, \quad (2)$$

where β is the half-width of the diffraction peak (FWHM), λ is the wavelength of X-rays, k is a constant (value equal to 1) which determines the shape of the reciprocal lattice point, D is the average size of the crystallite, and ε is a microstrain. Figure 4 shows the Williamson–Hall plot for three samples synthesized in this work.

Ni-7 min sample showed downward slope and then up, indicating the expansion and contraction of the lattice. Ni-12 min showed a linear pattern, a homogeneous behavior, i.e., it has approximately the same crystallite size. Therefore, the loss of homogeneity of the sample is due to the absence of linear pattern (Williamson and Hall 1953). The positive slope of the line indicates expansion of the crystal lattice (microstrain positive). Ni-17 min showed downward slope (microstrain negative), which is due to the contraction in the crystal lattice. The crystallite size and microstrain values were calculated, and are shown in Table 1. It was not possible to obtain the results of crystallite size for Ni-7 min, since this sample has presented a very high value for microstrain (Table 1). It could be also observed by linear correlation coefficients for the samples Ni-7 min (0.8275), Ni-12 min (0.9992), and Ni-17 min (−0.9691).

It was necessary to spend only two minutes to reach 160 °C in the synthesis of the nanoparticles. Despite this abrupt heating, typical of the microwave, very small crystals were obtained. This high rate of heating causes nucleation and growth regimes, which happens with different kinetics, resulting in the formation of a higher density of nuclei and particles of smaller size (Table 1). We note that the fast heating leads to smaller crystallite sizes and higher microstrain values,

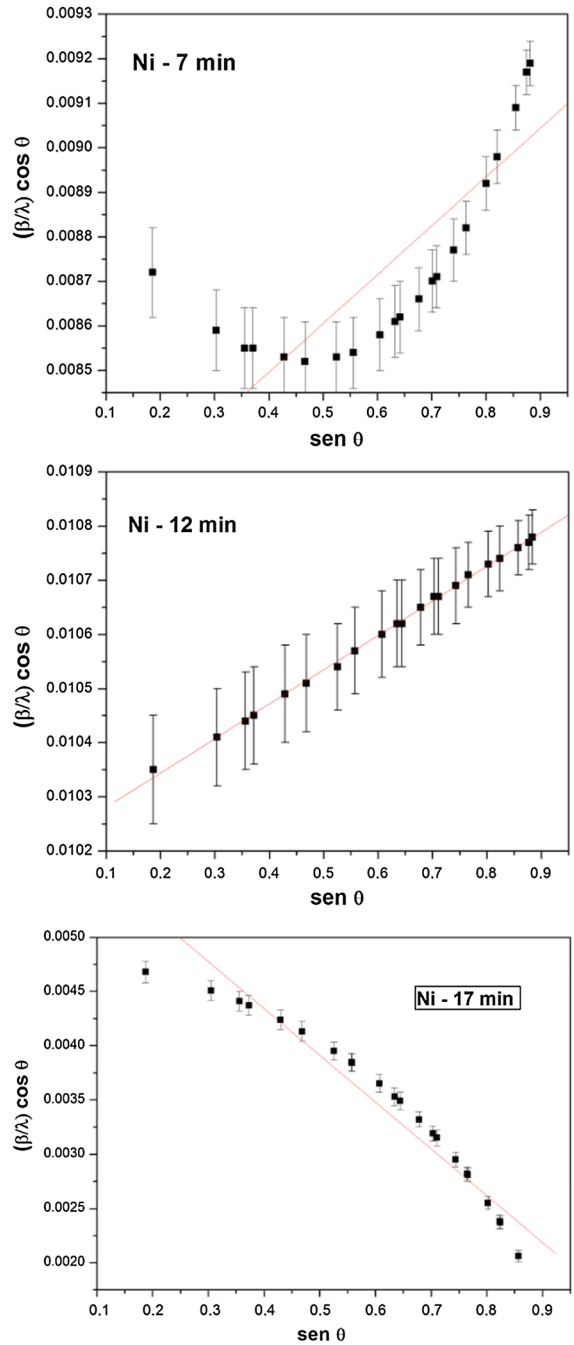

Fig. 4 Williamson–hall graphic of the samples

as we can see by the sample synthesized in 7 min. However, it presented a great disorder in their crystal structure. For this sample, the value of crystallite size remains virtually unchanged until the 12 min of heating. This means that the energy supplied was being used to homogenize the crystals, causing the

atoms occupy a position of thermodynamic equilibrium. It can be also evidenced by the decrease in the value of microstrain after 12 min. A striking difference between the microwave heating and conventional heating, using infrared radiation, must be precisely the sudden heating promoted by microwave radiation.

Figure 5 shows the ^{57}Fe Mössbauer spectra for nanoparticles. The probability distribution for the quadrupole interaction (Δ) values is also shown beside each spectrum. The experimental data are represented by black dots, while the red line denotes the adjustment made with the aid of the NORMOS program. The yellow and blue lines represent sub-spectra. Two sub-spectra can be observed for each sample, showing the iron occupation in two chemical environments, octahedral and tetrahedral sites. Δ for Ni-7 min indicated that Fe^{+3} ions have a preferential distribution, probably the octahedral site, typical for the spinel ferrites. It was also observed an evidence of migration of ions from one to another site with increasing of heating time. A doublet was observed for all samples, and it can be attributed to the occupation of Fe^{+3} ions in extremely small-sized particles, which exhibit superparamagnetic phenomenon (Amer et al. 2005). This pattern can be attributed to the collapse of the magnetic ordering, evidencing superparamagnetic character for all samples (Wang and Li 2001). The isomeric shift values were between 0.33 and 0.34 mm/s. According to literature (Dickson and Berry 1986), values in the range 0.1–0.5 mm/s are relative to iron with high-spin Fe^{3+} state. A positive shift indicates that s-electron density at the nucleus becomes more shielded because of larger number of d-electrons (Gibb 1994).

VSM analysis was performed to investigate the magnetic properties. Figure 6 shows magnetization loops of the nanoparticles at the temperatures of 300 and 5 K. Black curve shows the adjustment made using the Langevin function. The magnetic moments of the nanoparticles saturated quickly in the presence of an externally applied magnetic field (H). It was not observed the hysteresis behavior for the samples measured at 300 K (Fig. 6a), and this is the characteristic signature of superparamagnetic nanoparticles. This means that the nanoparticles have essentially single domain. It is possible to calculate its magnetization through the Langevin function (Yamaura et al. 2004). The values are presented in Table 2.

It was noticed that the saturation magnetization increases progressively with increasing particle size. This was due to the phenomenon that occurs on the surface which is due to the lack of translational symmetry at outer boundaries of a particle, reduced

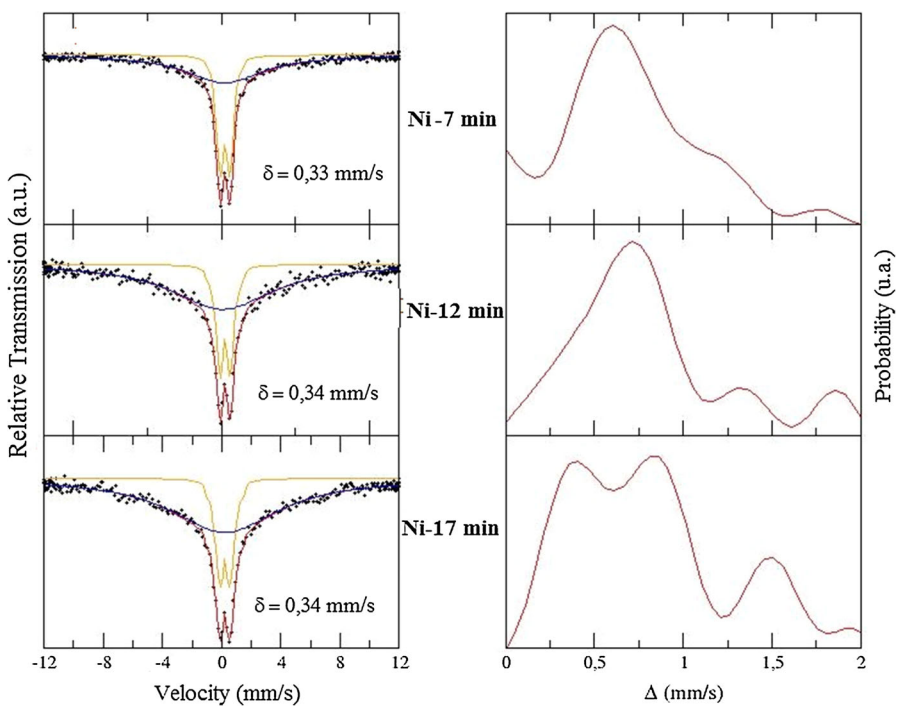

Fig. 5 ^{57}Fe Mössbauer spectrum of the magnetic nanoparticles

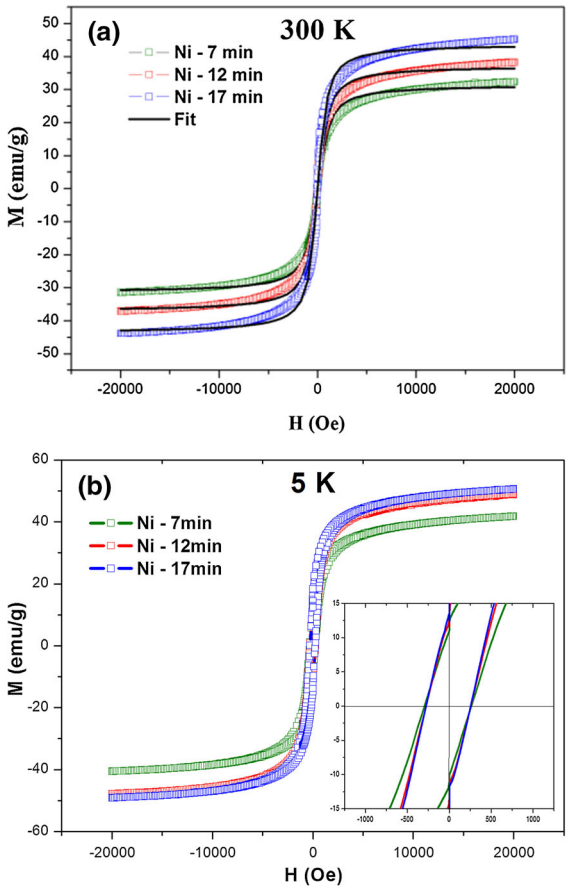

Fig. 6 Magnetization curves of the samples

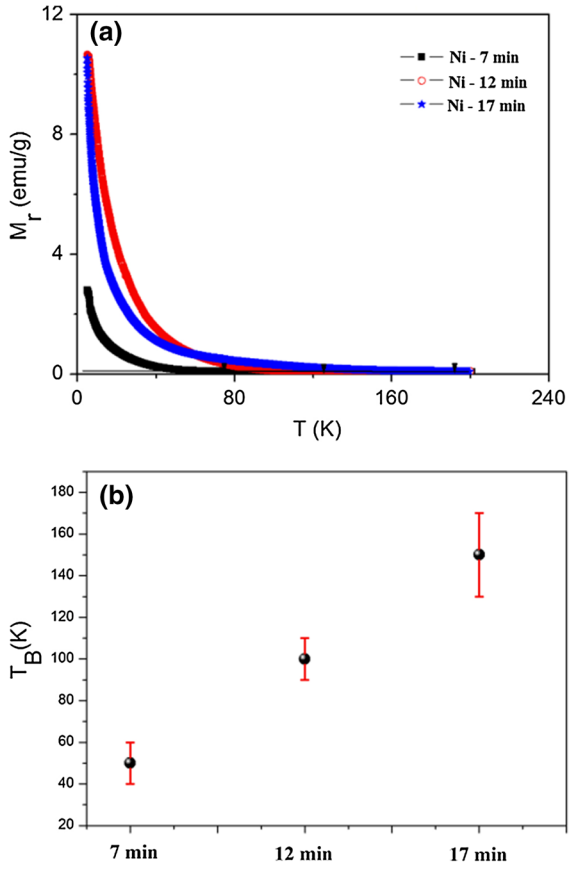

Fig. 7 **a** Remanent magnetization as a function of temperature. **b** Blocking temperature for samples Ni-7 min, Ni-12 min, and Ni-17 min

Table 2 Saturation magnetization (Ms), remanent magnetization (Mr), and coercivity field (Hc)

Samples	Ms (emu/g)	Mr (emu/g)	Hc (Oe)
T = 300 K			
Ni—7 min	32.4	–	–
Ni—12 min	38.3	–	–
Ni—17 min	45.2	–	–
T = 5 K			
Ni—7 min	41.8	12.0	276.8
Ni—12 min	48.8	12.3	260.3
Ni—17 min	50.6	18.4	257.0

coordination number, and broken magnetic exchange bonds of surface atoms. There is a region of approximately one nanometer on the surface that does not have magnetic phenomenon, i.e., not lined up in favor of an H. As the particle size increases, the value of the surface/volume ratio decreases. Thus, synthesized samples to high temperatures have a large size distribution of crystals consisting of multi-domains, resulting in a gain of magnetism (Freire et al. 2013).

Analyzing the magnetization curves obtained at 5 K (Fig. 6b), it was noticed the occurrence of hysteresis. Therefore, the values of M_s and H_c are shown to be non-zero. The loss of superparamagnetic behavior for all samples by the decreasing of the temperature can be described by the equation of relaxation time:

$$\tau = \tau_o \exp\left(\frac{KV}{k_B T}\right). \quad (3)$$

When magnetic particles are distributed in the nano-size range, the magnetic anisotropy barrier (KV) is smaller than the average thermal energy (k_BT) of the particles. Due to very small relaxation time (s), the magnetic moment flips rapidly, so that the effective

moment during the time of measurement becomes zero (KV/k_BT). This causes the collapse of a multiplet to a superparamagnetic doublet (Cullity and Graham 2011). At room temperature, the thermal energy is sufficient to cause inversion of spin as a function of H. As the temperature of the system reduces, the energy available to cause inversion of the spins also decreases, and some of the spins do not have an immediate response to change in the direction of the external magnetic field. Such behavior translates into loss of magnetization and the appearance of hysteresis in the curve. It is called blocking temperature (T_B). The temperature at which this phenomenon occurs and limits the separation between the two graphs is shown in Fig. 7, i.e., the temperature limit for the occurrence of loss of superparamagnetic behavior. This temperature can be estimated from Eq. 3, matching the relaxation time τ with a measurement time t_m typical of magnetization measurements, 100 s, for example, where we obtained the expression $T_B = KV/25\ k$, which depends on the volume (V) and anisotropy constant (K) of magnetic nanoparticles (Cullity and Graham 2011). T_B is found by plotting a graph of temperature as a function of remanent magnetization (M_r), (Fig. 7b).

Conclusions

Superparamagnetic nanoparticles of $NiFe_2O_4$ were obtained by hydrothermal process assisted by microwave heating. The mild conditions (time and temperature) found to synthesize nanoparticles were 140 °C/7 min (200 psi and 200 W). For instance, no spinel phase was observed for sample synthesized at 130 °C. This was confirmed by XRPD data. In order to extract as much as possible information from XRPD, refinement using the Rietveld method was performed. It was possible to observe that nanoparticles possess a high degree of crystallinity with crystallite size in the range of 9–15 nm. The crystallite size was found to increase with the heating time. TEM showed cubic shape for nanoparticles synthesized. The Mössbauer spectroscopy revealed superparamagnetic behavior for the samples synthesized. Moreover, it was observed the cationic mobility of the ions Fe^{3+} with the increase of the heating time. According to Mössbauer spectroscopy, VSM also showed superparamagnetic behavior with saturation of magnetization values in the range 32–46 emu/g for the samples at 300 K.

Acknowledgments This work was partly sponsored by CAPES, CNPq, and FUNCAP (Brazilian agencies). The support from Fondecyt 1140195, Millennium Science Nucleus, Basic and Applied Magnetism Grant N°P10-061-F, and CONICYT BASAL CEDENNA FB0807 is gratefully acknowledged (Chilean agencies). The authors acknowledge the Laboratório Nacional de Nanotecnologia (LNNano/CNPEM) for providing the equipment and technical support for the experiments involving transmission electron microscopy (TEM).

References

Amer MA, Meaz TM et al (2005) Mössbauer, infrared and X-ray studies of Ni0.5Zn0.5CrxFe2-xO4 ferrites. Egyp J Solids 28:3

Barreto A, Santiago V et al (2011) Magnetic nanoparticles for a new drug delivery system to control quercetin releasing for cancer chemotherapy. J Nanopart Res 13(12):6545–6553

Bennett CO, Myers JE (1982) Momentum, heat, and mass transfer. McGraw-Hill, New York

Bleicher L, Sasaki JM et al (2000) Development of a graphical interface for the Rietveld refinement program DBWS. J Appl Crystallogr 33(4):1189

Braga TP, Vasconcelos IF et al (2010) Magnetic composites based on hybrid spheres of aluminum oxide and superparamagnetic nanoparticles of iron oxides. J Magn Magn Mater 322(6):633–637

Cullity BD, Graham CD (2011) Introduction to magnetic materials. Wiley, New York

Dickson DPE, Berry FJ (1986) Mössbauer spectroscopy. Cambridge University Press, Cambridge

Freire R, Ribeiro T et al (2013) MZnFe2O4 (M=Ni, Mn) cubic superparamagnetic nanoparticles obtained by hydrothermal synthesis. J Nanopart Res 15(5):1–12

Friedlander SK (2000) Smoke, dust, and haze. Oxford University Press, New York

Gibb TC (1994) Encyclopedia of Inorganic Chemistry. Wiley, Chidrester

Karakas ZK, Boncukcuoglu R et al (2013) The Investigation of the Removal of the Arsenic from Wastewaters by Using NiFe2O4 Nanoparticles Produced with Microwave Assisted Combustion Method. J Selcuk Univ Nat Appl Sci 2013:332–338

Klabunde KJ, Richards R (2001) Nanoscale materials in chemistry. Wiley, New York

Koziej D, Floryan C et al (2013) Microwave dielectric heating of non-aqueous droplets in a microfluidic device for nanoparticle synthesis. Nanoscale 5(12):5468–5475

Latham AH, Williams ME (2008) Controlling Transport and Chemical Functionality of Magnetic Nanoparticles. Acc Chem Res 41(3):411–420

Markov IV (1995) Crystal growth for beginners: fundamentals of nucleation, crystal growth, and epitaxy. World Scientific, Singapore

Patterson A (1939) The Scherrer formula for X-ray particle size determination. Phys Rev 56(10):978

Petcharoen K, Sirivat A (2012) Synthesis and characterization of magnetite nanoparticles via the chemical co-precipitation method. Mater Sci Eng, B 177(5):421–427

Rietveld HM (1967) Line profiles of neutron powder-diffraction peaks for structure refinement. Acta Crystallography 22:151–152

Thomas JJ, Shinde AB, Krishna PSR, Kalarikkal N (2013) Cation distribution and micro level magnetic alignments in the nanosized nickel zinc ferrite. J Alloy Compd 546:77–83. doi:10.1016/j.jallcom.2012.08.011

Tong J, Cai X et al (2013) Efficient magnetic CoFe2O4 nanocrystal catalyst for aerobic oxidation of cyclohexane prepared by sol–gel auto-combustion method: effects of catalyst preparation parameters. J Sol-Gel Sci Technol 66(3):452–459

Wang L, Li FS (2001) Mossbauer study of nanocrystalline Ni-Zn ferrite. J Magn Magn Mater 223(3):233–237

Weidler P, Luster J et al (1998) The Rietveld method applied to the quantitative mineralogical and chemical analysis of a ferralitic soil. Eur J Soil Sci 49(1):95–105

Williamson G, Hall W (1953) X-ray line broadening from filed aluminium and wolfram. Acta Metall 1(1):22–31

Yamaura M, Camilo R et al (2004) Preparation and characterization of (3-aminopropyl) triethoxysilane-coated magnetite nanoparticles. J Magn Magn Mater 279(2):210–217

Zhang Z-G, YAO G-C et al (2010) Synthesis of NiFe2O4 spinel nanopowder via low-temperature solid-state reactions. J Northeastern Univ (Nat Sci) 31(6):868–872

Zhang W, Jia S et al (2012) Studies of the magnetic field intensity on the synthesis of chitosan-coated magnetite nanocomposites by co-precipitation method. Mater Sci Eng, C 32(2):381–384

Zhang W, Jia S-Y et al (2013) Effects of alkaline precipitating agents on synthesis of magnetite nanomaterials by hydrothermal D-glucose method. J Nanopart Res 15(6):1–6